Appl. Phys. A 80, 55–59 (2005)
DOI: 10.1007/s00339-004-3017-z

Applied Physics A
Materials Science & Processing

D. ELVERS[1]
L. REMER[1]
N. ARNOLD[2]
D. BÄUERLE[2,✉]

Laser microdissection of biological tissues: process optimization

[1] Leica Microsystems AG, 35578 Wetzlar, Germany
[2] Institut für Angewandte Physik, Johannes-Kepler-Universität, Altenbergerstrasse 69, 4040 Linz, Austria

Received: 29 July 2004 / Accepted: 6 August 2004
Published online: 21 September 2004 •

ABSTRACT The dynamical behavior of dissectats obtained in laser microdissection of biological tissues on polymer membranes can be semiquantitatively described by taking into account only the influences of gravity and friction. An important role is played by the initial velocity v_0 which is related to the momentum transfer onto the dissectats during laser ablation. From the analysis of data we suggest possibilities to increase the yield of dissectats collected in laser microdissection.

PACS 42.62.Be; 52.38.Mf; 79.20.Ds; 52.50.Jm; 87.80.-y

1 Introduction

Laser microdissection is a well-known technique for rapid preparation of small specimens from organic tissues for subsequent investigations in different areas of molecular biology and medicine. In this technique an optical microscope is used together with a laser beam for inspection of large-area samples and subsequent dissection of small specimens, so-called dissectats, which contain cells of particular interest for further investigations. The dissectats are collected in small vessels for histological investigations, cell surgery, gene analysis, etc. [1–7]. The samples typically employed consist of a microtome cut of the biological tissue placed on a supporting polymer foil. With the laser fluences typically used in microdissection instruments, dissection is mainly based on local laser-induced ablation. While the ablation of organic polymers at the laser wavelengths ($\lambda > 200$ nm) under consideration is based on mainly photothermal mechanisms, thermomechanical processes related to the expansion/evaporation of water play an important or even decisive role in laser ablation of biological tissues [8].

The application of lasers for the isolation of particular cells from composite tissues, but also for single-cell excitation, modification or decomposition, has many advantages. Laser techniques allow a high degree of versatility; they are fast and permit very high spatial and temporal resolution. Thus, short intense laser pulses permit very localized processing of heat-sensitive biological cells and tissues with minor damage of the surrounding material. For biological and medical applications it is also essential that laser beams are almost massless tools which are absolutely sterile. Finally, laser technology is completely compatible with present-day electronic- and computer-control techniques. In laser microdissection one of the main disadvantages is the relatively low yield of dissectats achieved with this technique. Here, a significant percentage of specimens gets lost after dissection. This may have various origins, depending on the particular setup employed in the investigations. The main reasons, however, are related to the undefined initial conditions after microdissection which strongly influence the hydrodynamic motion of the dissectats to the collecting vessel. In addition to the well-known hydrodynamic instabilities, density changes and convection within the ambient atmosphere may result in motions of the dissectats along complex trajectories that considerably deviate from a straight line directed from the sample to the collecting vessel. In experimental arrangements where the dissectat moves in a direction opposite to gravity, the dissectat may even reverse the motion and condense on the sample. Of minor importance with respect to the overall yield are cases where the dissectat gets stuck within the remaining hole of the sample.

In this paper we investigate the laser-microdissection process and the dynamics of the motion of dissectats by means of an ultra-fast camera. The experimental results are analyzed on the basis of model calculations. As a result of these investigations we suggest various improvements of the laser-microdissection process which significantly enhance the yield of dissectats achieved in this technique.

2 Experimental setup

The setup employed in the experiments is schematically shown in Fig. 1. The main components are a Leica AS LMD laser-microdissection system and a high-speed camera (SpeedCam Visario, Weinberger Inc., Germany). The Leica AS LMD system consists of a Leica DM LA microscope and a N_2 laser ($\lambda = 337.1$-nm UV-A radiation, pulse length $\tau_\ell \lesssim 4$ ns, repetition rate $\nu_\ell = 15$–60 pps). In this system, the laser beam is incident onto the sample from above, i.e. its direction of propagation, $\boldsymbol{k}$, is almost parallel to the vector of gravity, $\boldsymbol{g}$. This is schematically shown in Fig. 2a. Besides samples where the polymer foil with the biological tissue was mounted on a transparent glass support (samples of type 1),

✉ Fax: +43-732-2468-9242, E-mail: dieter.baeuerle@jku.at

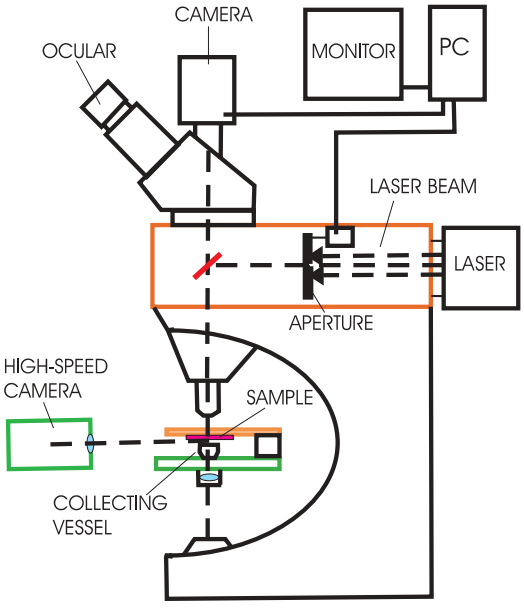

FIGURE 1 Schematic picture of the experimental setup. The Leica laser-microdissection system AS LMD consists of a Leica DM LA microscope and a N_2 laser. The dynamics of the laser-microdissection process was followed by means of a high-speed camera (SpeedCam Visario)

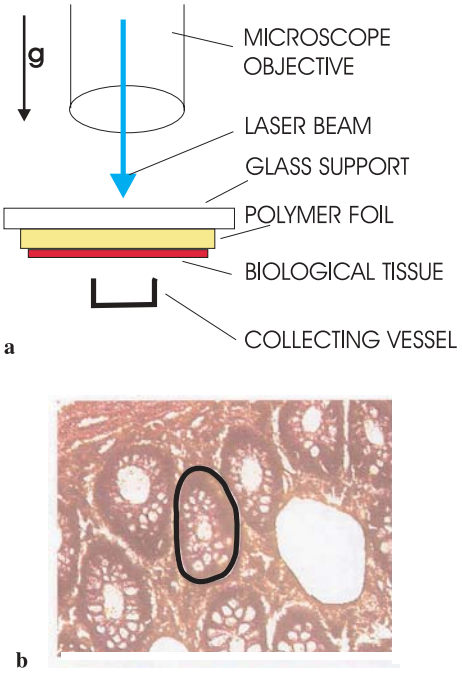

FIGURE 2 **a** Schematic of the irradiation geometry and orientation of a sample of type 1. ***g*** is the vector of gravity. With samples of type 2 the polymer foil is mounted in a frame without a glass support. **b** Example of a biological tissue on a polymer membrane. The *full curve* circumscribes the area of interest for laser microdissection. The *white area* is a hole in the sample from a previously dissected specimen. The tissue was stained with hematoxylin eosin. The length of the picture diagonal is 396 μm

we used samples where the polymer foil was mounted within a frame without a glass support (type 2). For samples of types 1 and 2 the polymer foils consisted of polyethylene naphthalene (PEN) and polyethylene terephthalate (PET, same as Mylar), respectively. After mounting on the microscope table, the sample can be inspected either via the ocular of the microscope or on a monitor (Fig. 1). After selection of a particular area of interest on the large-area tissue sample, a closed trajectory around this specimen (full curve in Fig. 2b) is chosen by using the standard Leica software. Subsequently, laser cutting along this trajectory is started. Here, the laser beam moves with respect to the fixed substrate. In the so-called Leica 'standard mode' the laser-light intensity is kept constant during the whole cutting process. In the 'combined mode', the overall intensity is changed by slightly increasing the aperture just before complete dissection of the specimen. After complete dissection, the dissectat falls down and is collected in a vessel below the sample.

The high-speed camera (SpeedCam Visario) contains a CMOS sensor. It permits a recording frequency of 1000 pictures per second with a resolution of 1536×1024 pixels. This camera was adjusted in such a way that the sample could be observed from below under a glancing angle. By this means, it was possible to observe both the dissection process itself and the motion of the dissectat towards the vessel.

3 Experimental results

Figure 3 shows a typical picture taken with the high-speed camera and a sample of type 1. For illustration, this picture shows both specimens before complete microdissection and a dissectat on its way to the collecting vessel. From this picture it becomes evident that specimens cut out from large-area samples peel off from the glass support before complete dissection. This effect is related to the momentum transfer during laser cutting and to thermomechanical strains which build up within the polymer foil during the dissection process.

The high-speed camera together with its software permits one to automatically detect the coordinates of the moving dissectat as a function of elapsed time. Thus, from a series of pictures of this type, the temporal behavior of the trajectory of the dissectat within xz planes can be determined with

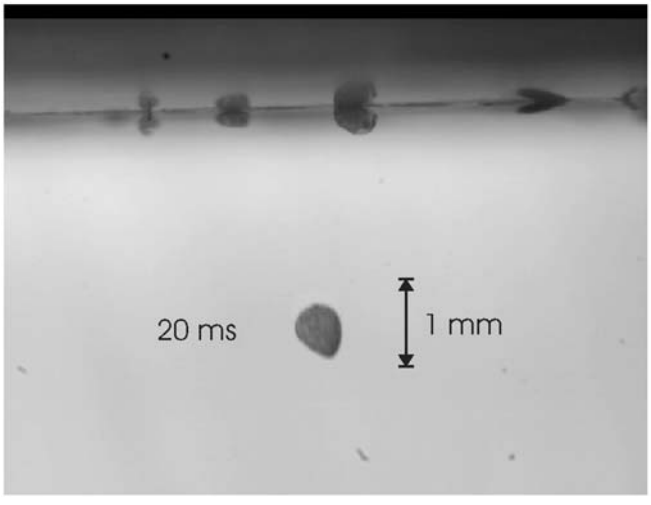

FIGURE 3 The picture taken with the high-speed camera shows both dissectats before complete microdissection (sample of type 1) and a single dissectat (diameter $d = 600$ μm) on its way to the collecting vessel. Note that dissectats peel off from the glass support before complete dissection (*upper part*). The flight time of the dissectat shown in the *lower part* was 20 ms

high precision. Figures 4a and 5a show $z = z(t)$ diagrams obtained in this way for disc-shaped dissectats with diameters of $d = 2r = 600\,\mu\text{m}$ and 50 μm, respectively. A behavior similar to that shown in Figs. 4 and 5 was observed for dissectats with diameters of 150 μm and 100 μm. Here, the radius of the laser spot on the sample surface was $w = 7.5\,\mu\text{m}$ for the 600-μm dissectats and $w = 1.5\,\mu\text{m}$ for all the other dissectats. In all experiments, the z direction was parallel to the vector of gravity, i.e. $z \parallel \boldsymbol{g}$. The diagrams reveal a number of interesting features: first, there is no systematic difference in the dynamic behavior of dissectats obtained in the Leica 'standard mode' and the 'combined mode'. Second, for short times t, the dynamics of dissectats changes significantly for subsequent microdissection experiments, even in cases where all of the experimental parameters were kept constant. Third, the velocity of dissectats $v \equiv \dot{z}(t) = \mathrm{d}z/\mathrm{d}t$ for times $t \to 0$ increases with decreasing diameter d.

Figure 6 shows the velocity of dissectats at a late stage of descent as a function of their diameter. Though the longest time intervals, $t^{\max}$, investigated in the present experiments were finite, this velocity should be close to the terminal velocity v_∞. The figure reveals that the velocities v_∞ obtained for samples of type 1 systematically exceed those obtained for samples of type 2. This may be related to the observation that dissectats obtained from samples of type 1 show both a higher initial velocity v_0 and a stronger rotation during the motion.

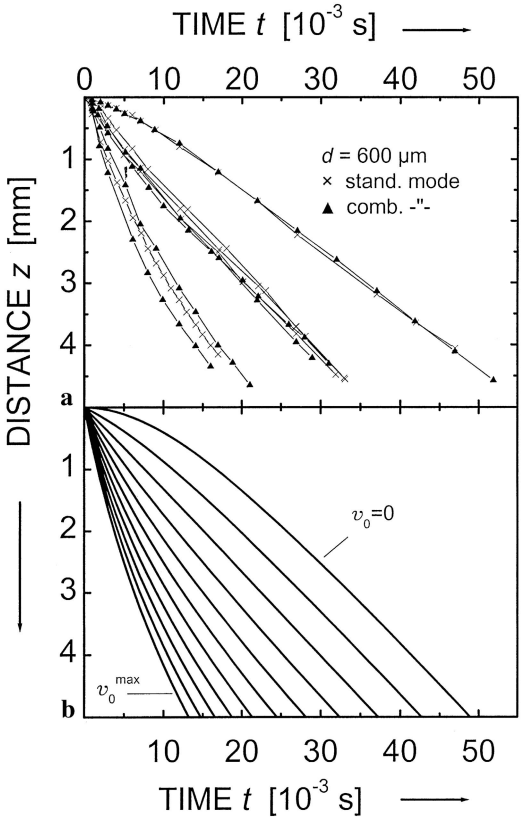

FIGURE 4 Dynamic behavior of dissectats of diameter $d = 600\,\mu\text{m}$ dissected from samples of type 1. **a** The experimental data were obtained with either the Leica standard mode (×) or the combined mode (▲). **b** Curves calculated from (1)

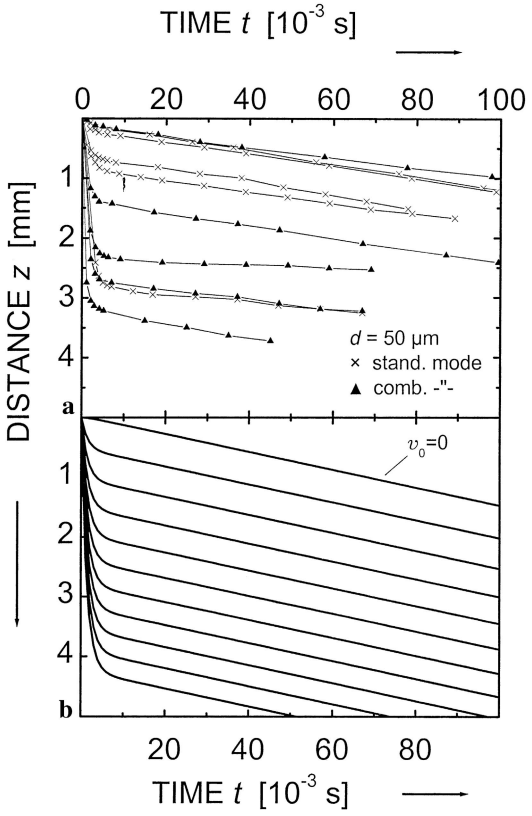

FIGURE 5 Same as in Fig. 4 but for dissectats of diameter $d = 50\,\mu\text{m}$

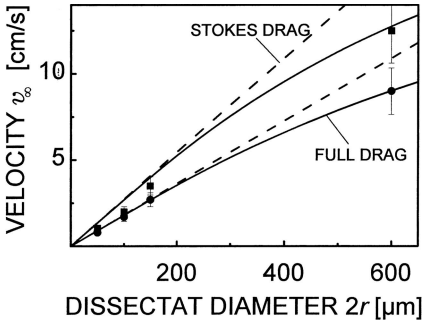

FIGURE 6 Terminal velocity v_∞ as a function of the diameter of dissectats. The symbols ■ and • refer to experimental values obtained for samples of type 1 (polymer over glass) and type 2, respectively. The *full curves* were calculated from (4). The *dashed curves* were obtained by taking into account only Stokes friction ($\delta = 0$). In the analysis we used for the data ■ the drag coefficients $\gamma = 32\eta r/3$ and $\delta = 1.18r^2\varrho_g$, while for the data • $\gamma = 16\eta r$ and $\delta = 1.18\pi r^2\varrho_g/2$ have been employed

The following analysis reveals that most of these observations can be explained on the basis of simple model calculations which take into account the very different initial conditions related to the laser-microdissection process.

4 Dynamics of dissectats

In the simplest approximation the dynamics of dissectats of mass m can be described by the differential equation $m\ddot{z}(t) + \gamma\dot{z}(t) + \delta\dot{z}^2 = mg$. Here, the second and third terms describe Stokes and Newtonian friction forces, respectively. The description of the total hydrodynamic drag by the sum of

viscous and inertial drag forces is a good approximation over a wide range of Reynolds numbers. For circular discs moving in directions $\boldsymbol{v} \parallel \hat{\boldsymbol{n}}$, the drag coefficient γ can be described by $\gamma \approx 16\eta r$. Here, $\hat{\boldsymbol{n}}$ is the surface normal onto the dissectat. For motions $\boldsymbol{v} \perp \hat{n}$ the approximation $\gamma = 32\eta r/3$ can be employed [9]. η is the dynamic viscosity, which is given by $\eta = \nu \varrho_g = 1.8 \times 10^{-4}\,\mathrm{g/cm\,s}$. For air at normal conditions the kinematic viscosity is $\nu = 0.15\,\mathrm{cm^2/s}$ and the density $\varrho_g = 1.23 \times 10^{-3}\,\mathrm{g/cm^3}$. The drag coefficient δ can be described, approximately, by $\delta \approx 1.18\pi r^2 \varrho_g/2$ if $\boldsymbol{v} \equiv v_z \parallel \hat{\boldsymbol{n}}$ [10]. The solution of the equation of motion is

$$z = \frac{m}{\delta} \ln \left\{ \cosh \left[\frac{\gamma}{2m} \sqrt{1 + \frac{4mg\delta}{\gamma^2}}\, t \right] + \frac{v_0 + \dfrac{\gamma}{2\delta}}{\dfrac{\gamma}{2\delta}\sqrt{1 + \dfrac{4mg\delta}{\gamma^2}}} \sinh \left[\frac{\gamma}{2m} \sqrt{1 + \frac{4mg\delta}{\gamma^2}}\, t \right] \right\} - \frac{\gamma}{2\delta} t. \tag{1}$$

This solution satisfies the initial conditions $z(0) = 0$ and $\dot{z}(0) = v_0$. With low velocities we can ignore Newtonian friction and use the approximation $\delta \approx 0$. We then obtain

$$z(t) \approx \frac{m}{\gamma} \left(v_0 - \frac{mg}{\gamma} \right) \left\{ 1 - \exp\left(-\frac{\gamma}{m} t \right) \right\} + \frac{mg}{\gamma} t. \tag{2}$$

An important quantity in these solutions is the initial velocity of dissectats after dissection, v_0. This velocity is closely related to the laser-ablation process. Let us consider normal incidence of the laser beam which, for the Leica system and the diameters of dissectats under consideration, is a very good approximation. For samples of type 2, the laser-induced plasma propagates towards the incident laser beam, i.e. in a direction opposite to $\boldsymbol{k}$. This causes a recoil pressure onto the dissectat in the $\boldsymbol{k}$ direction $\parallel \boldsymbol{g}$. The momentum transfer related to this pressure can be approximated by $mv_0 \approx m_v v_v$, where m_v and v_v are the mass and the velocity of ablated species, respectively. For samples of type 1, the situation is somewhat more complicated. Here, free expansion of the plasma is suppressed by the glass support. Thus, a considerable number of ablated species is trapped between the polymer foil and the glass. As a consequence, besides the recoil pressure related to the ablation process, we have to consider also the thermal pressure that is related to the dissipation of the kinetic energy of plasma species. The contribution of this additional pressure to the velocity v_0 may tentatively explain the somewhat higher initial velocities of dissectats observed for samples of type 1. It can be estimated from $mv_0^2 = \zeta m_v v_v^2$ with $0 \le \zeta \le 1$. Here, ζ is a very complex quantity. It depends on the sticking coefficients of species on the glass support and the polymer membrane, the thermal conductivities of materials and, importantly, on the progression of the dissection process. As already mentioned in connection with Fig. 3, the dissectats peel off from the support before complete microdissection. Thus, during dissection, an increasing number of ablated species can escape from the volume of interaction.

In any case, v_0 is within the range $0 \lesssim v_0 \lesssim v_0^{\max}$. The lower and upper limits are mainly determined by the width of the remaining bridge before the final laser shot, i.e. before complete dissection. If the width of this bridge is very small, the ablated mass m_v, and thereby the momentum transfer to the dissectat, is small. If the width of this bridge is approximately equal to the size of the laser spot, the ablated mass, and thereby the momentum transfer onto the dissectat during the final laser shot, is maximum. Thus, with setups usually employed in laser microdissection, the value of this initial velocity v_0 changes arbitrarily between the limits $v_0 \gtrsim 0$ and $v_0^{\max}$. It depends on whether the length of the trajectory selected in a particular experiment contains an integral number of laser spot sizes $2w$ or not.

5 Numerical calculations

Figures 4b and 5b show the behavior of the function $z = z(t)$ calculated from (1). The following parameters have been employed: the density and the thickness of the polymer foil were $\varrho_\mathrm{p} = 1.35\,\mathrm{g/cm^3}$ and $h_\mathrm{p} = 1.5\,\mu\mathrm{m}$, respectively. For the average density and the thickness of the tissue we used $\varrho = 0.8\,\mathrm{g/cm^3}$ and $h = 1.8\,\mu\mathrm{m}$, respectively (for the estimation of ϱ and h, the loss of water and the incomplete coverage of the polymer foils by the particular tissue samples were taken into account). The mass of dissectats is $m = \pi r^2(\varrho_\mathrm{p} h_\mathrm{p} + \varrho h)$. The maximum mass of the ablated material is given by $m_v = \pi w^2(\varrho_\mathrm{p} h_\mathrm{p} + \varrho h)$, where $2w$ is the width of the laser spot on the sample surface. Henceforth, we use the approximation $m_v \approx \pi w^2 \varrho_\mathrm{p} h_\mathrm{p}$. Thus, we have assumed that with the particular tissue employed, v_0 is mainly determined by the momentum transfer caused by the ablation of the polymer membrane only. Typical values of the velocity of ablated species are $v_v \approx 2.9 \times 10^5\,\mathrm{cm/s}$ [8].

The different curves in Figs. 4b and 5b correspond to different initial velocities v_0 calculated in steps of $v_0 = i v_0^{\max}/n$. The case $i = 0$ yields, in the initial phase, a parabola, as expected for the free fall. For $i = n$, the slope of the curves for $z, t \to 0$ is maximum. This slope is steeper for small dissectats. The maximum velocity $v_0^{\max}$ was calculated from $mv_0^{\max} = m_v v_v$. With these parameters employed in the calculations, we obtain for dissectats of diameter $d = 600\,\mu\mathrm{m}$ a maximum velocity $v_0^{\max} = 64\,\mu\mathrm{m/s}$ and a Reynolds number $\mathcal{R}e \equiv 2v_0 r/\nu \approx 26$. For dissectats of diameter $d = 50\,\mu\mathrm{m}$ the corresponding values are $v_0^{\max} = 371\,\mathrm{cm/s}$ and $\mathcal{R}e \approx 12$. The comparison of the curves $z = z(t)$ calculated from (1) with those calculated from (2) reveals that Newtonian drag plays a much more important role in the initial phase of motion and for velocities $v_0 \approx v_0^{\max}$. If we take into account the ablation of the biological tissue in the same way as that of the polymer foil, the velocity v_0 becomes much higher. Qualitatively, however, the overall shape of the curves and the influence of v_0 remain the same.

The time of transition from 'fast' motion to 'slow' motion with $\dot{z} \equiv v_z\,(t \to \infty) \equiv v_\infty = \mathrm{const}$ is reached much earlier for small dissectats. It can be estimated from

$$t_\infty = \left[\frac{\gamma}{2m}\sqrt{1+\frac{4mg\delta}{\gamma^2}}\right]^{-1} . \quad (3)$$

Note that the coefficients γ and δ depend on the size and shape of dissectats and on their orientation during falling. From (1) we obtain the terminal velocity

$$v_\infty = \frac{\gamma}{2\delta}\left(\sqrt{1+\frac{4mg\delta}{\gamma^2}}-1\right) = C_1\frac{\eta}{\varrho_g \pi r}\left(\sqrt{1+C_2\frac{(\varrho h+\varrho_\mathrm{p}h_\mathrm{p})g\varrho_g}{\eta^2}r^2}-1\right), \quad (4)$$

where C_1 and C_2 are constants. The dependence of v_∞ calculated from (4) as a function of the diameter of dissectats is included in Fig. 6 by the solid curves. The analysis reveals that Newtonian friction influences the terminal velocity v_∞ mainly for large dissectats. For very small dissectats we can use the approximation $\delta \to 0$ and obtain from (2) or (4)

$$v_\infty = \frac{mg}{\gamma} = C_3\frac{(\varrho h+\varrho_\mathrm{p}h_\mathrm{p})g}{\eta}r \quad (5)$$

Here C_3 is again a constant. For motions of circular dissectats with $\boldsymbol{v} \parallel \hat{\boldsymbol{n}}$, we have $C_1 = 16/1.18$, $C_2 = 1.18\pi^2/128$ and $C_3 = \pi/16$.

In this approximation the velocity v_∞ increases linearly with the diameter of dissectats (dashed lines). This is in agreement with the measurements for small dissectats. With the parameter set employed in the present calculations, the influence of Newtonian friction can be observed only for dissectat diameters $d \gtrsim 300\,\mu\mathrm{m}$. The fact that the data obtained for samples of type 1 systematically exceed those for samples of type 2 is not fully understood. As already mentioned, it may be related to the higher initial velocity v_0 and the stronger rotation of these dissectats. This stronger rotation of dissectats obtained from samples of type 1 was observed even for the longest times investigated, t_max. This observation is in contrast to the simple picture that in late stages of descent of dissectats the stable orientation is $v \equiv v_z \parallel \hat{n}$. Apparently, the dynamics of falling dissectats is much more complex. There seem to exist different distinct types of motion. In fact, such different types of motion of falling discs and strips have been recently investigated and mapped in 'phase diagrams' [11, 12]. Such an analysis is certainly beyond the scope of this paper. Instead, we take into account the strong rotation of dissectats from samples of type 1 by using smaller drag coefficients γ and δ. Namely, instead of $\gamma = 16\eta r$ we use $\gamma = 32\eta r/3$, which corresponds to the smallest possible value for $\boldsymbol{v} \perp \hat{\boldsymbol{n}}$. As no exact expressions for the drag force on a rotating object exist, we multiply $\delta = 1.18\pi r^2\varrho_g/2$ by the average cosine value $2/\pi$, so that $\delta = 1.18r^2\varrho_g$. The upper curves in Fig. 6 have been calculated in this way.

6 Discussion

The comparison of Fig. 4a, b and Fig. 5a, b shows that the dynamical behavior of dissectats obtained in laser microdissection can be semiquantitatively described on the basis of Newton's equation by taking into account only the influences of gravity and friction. The strong differences in the shape of the curves $z = z(t)$ obtained in consecutive experiments performed with constant experimental parameters is related to the different initial conditions which determine the velocity v_0. With velocities $v_0 \approx 0$ the curves start with a relatively flat slope, while with $v_0 \approx v_0^\mathrm{max}$ this slope is quite steep. Thus, the initial velocity v_0 strongly determines the subsequent motion of dissectats. From the previous analysis we find that this influence can be very pronounced over distances $\ell \lesssim v_0 t_\infty$. Thus, the distances between the samples and the collecting vessels employed in laser microdissection should not exceed ℓ. Note that t_∞, and therefore ℓ, depend on the size of dissectats. This is in agreement with the experimental results in Figs. 4 and 5. For example, with 600-μm dissectats, the flight time to the collecting vessel at a distance of 5 mm changes by a factor of two to five, depending on v_0. For small dissectats this influence is much stronger. With 50-μm dissectats and small velocities v_0, the dissectats may laterally drift away before reaching the collecting vessel. Thus, for increasing the yields of dissectats achieved in laser-microdissection equipments of the Leica type, it is advantageous to maximize the initial velocity v_0 in the z direction. By this means, the dissectats reach the collecting vessel much faster. External disturbances on the motion of dissectats become less important. This can be achieved by controlling the cutting process along the selected trajectory (see Fig. 2b) in such a way that the width of the bridge before the last laser shot, i.e. before complete dissection, becomes approximately equal to the diameter of the laser spot. By this means, the initial velocity of dissectats in subsequent experiments will always be around $v_0 \approx v_0^\mathrm{max}$. It is evident that the mass of ablated material, and thereby v_0^max, also increases with increasing thickness of the polymer foil, h_p, and with increasing width of the laser spot size, $2w$. Certainly, whether h_p and/or $2w$ can be increased in an experiment depends on the particular problem under investigation.

REFERENCES

1 F. Hillenkamp, R. Kaufmann, E. Remy: Laser Angew. Strahlentech. **4**, 40 (1971); W. Meier-Ruge, W. Bielser, E. Remy, F. Hillenkamp, R. Nitsche, R. Unsold: Histochem. J. **8**, 387 (1976)
2 G. Isenberg, W. Bielser, W. Meier-Ruge, E. Remy: J. Microsc. **107**, 19 (1976)
3 Y. Kubo, F. Klimek, Y. Kikuchi, P. Bannasch, O. Hino: Cancer Res. **55**, 989 (1995)
4 *Leica AS LMD Users Manual* (2003)
5 K. Schütze, G. Lahr: Nat. Biotechnol. **16**, 737 (1998)
6 L. Cerroni, G. Minkus, B. Pütz, H. Höfler, K. Kerl: Br. J. Dermatol. **136**, 743 (1997)
7 M. Ganser, A. Weiß, J. Wesner, G. Johannsen: German Patent No. DE 10 043 506 C1 (2001)
8 D. Bäuerle: *Laser Processing and Chemistry*, 3rd edn. (Springer, Berlin 2000)
9 L.D. Landau, E.M. Lifschitz: *Course of Theoretical Physics, Vol. VI, Fluid Mechanics* (Pergamon, New York 1987)
10 R.L. Street, J.K. Vennard, G.Z. Watters: *Elementary Fluid Mechanics* (Wiley, New York 1995)
11 S.B. Field, M. Klaus, M.G. Moore, F. Nori: Nature **388**, 252 (1997)
12 A. Belmonte, H. Eisenberg, E. Moses: Phys. Rev. Lett. **81**, 345 (1998)